Journal of Mining and Environment (JME) Vol. 17, No. 3, 2026, 847-864

Shahrood University of Technology

Journal of Mining and Environment (JME)

Journal homepage: www.jme.shahroodut.ac.ir

Iranian Society of Mining Engineering (IRSME)

Cooperative Mining of Overlying Section Coal Pillars in Steeply Inclined and Extremely Close Coal Seams: A numerical investigation

Feng Yang[1], Pengjie Li[1]*, and Qiang Sun[1,2]

1. School of Mines, China University of Mining & Technology, Xuzhou 221116, China
2. State Key Laboratory for Geomechanics and Deep Underground Engineering, China University of Mining & Technology, Xuzhou 221116, China

Article Info

Received 30 July 2025
Received in Revised form 12 October 2025
Accepted 10 January 2026
Published online 10 January 2026

DOI: 10.22044/jme.2026.16570.3246

Keywords

Fly ash
Bentonite, Glass fibre
Unconfined compressive strength
Coefficient of permeability

Abstract

Large coal pillars result in significant resource waste. The high stress concentration within these pillars also creates safety hazards for the working face. To address this, a cooperative mining method for section coal pillars is proposed. This method is designed for seams with large inclination angles and that are extremely close to overlying pillars. The technical principles are explained. First, FLAC3D simulation software was used to investigate the effect of the spacing between the lower roadway and the section coal pillar, which determined the optimal roadway position. Then, a coupled FLAC-PFC method was employed to optimize the coal drawing process parameters. The optimal scheme was analyzed to characterize roof deformation, stress distribution, and hydraulic support loads. An engineering case study demonstrates that a spacing greater than 18 m minimizes the influence of concentrated stress, resulting in limited deformation and improved roadway stability. The study investigates coal drawing under different sequences, port widths, and methods. The optimal process was identified as downward drawing, with a 1.5 m coal drawing port width and a two-wheel sequential method. This process achieves a drawing rate of 85.62% and a gangue content of 4.61%. Analysis shows that during the pillar drawing process, the concentrated stress on the roof plate is significantly reduced, with a maximum stress decrease of 21.1 MPa, effectively alleviating stress concentration. The total force on the section hydraulic support in fully mechanized caving is 1.6×10^4 kN, while the force in the fully mechanized mining section is 1.4×10^4 kN.

1. Introduction

Coal is a primary energy source for China and many other countries. Its core status in the energy supply will remain stable for the foreseeable future. In recent years, as shallow and easily accessible coal resources in eastern China are gradually depleted, the focus of coal development has shifted westward. However, geological conditions in the western regions are complex. These deposits often feature large dip angles, thick or extra-thick seams, and closely spaced seam groups, which significantly increase the difficulty of extraction. At the same time, continued mining operations intensify rock mass disturbances, leading to severe ground pressure phenomena that pose serious challenges to mine safety. Leaving section pillars is a common technical method to address mining under high stress, weak rock, and special geological conditions. However, this practice not only wastes significant coal resources but can also leave behind safety hazards for future working faces [1-5].

Researchers have extensively studied the issue of coal pillar stability from multiple perspectives. For example, using probabilistic methods such as Monte Carlo simulation to assess the stability of chain pillars has become an important approach [6]. Ghasemi et al. have developed intelligent methods to predict the size of pillars in room-and-pillar mining and the overall stability of mines [7,8], as well as techniques like stacked

Corresponding author: lipengjie@cumt.edu.cn (P. Li)

generalization to predict the stability status of hard rock pillars [9]. The study of pillar failure mechanisms is also in-depth, including the analysis of the failure process of rock pillars containing non-persistent joints or edge notches through experiments and numerical simulations [10,11]. Furthermore, factors such as coalbed gas emissions [12] and the adsorption of carbon dioxide and methane on the mechanical properties of coal and pillar stability have also received attention [13]. Meanwhile, new analytical methods, such as using the Coulomb graphical method to analyze the stability of chain pillars in longwall mining, are continuously being proposed [14]. Compared to single-seam mining, the roof structure evolution and stress distribution in extremely close-proximity seams are distinct, classifying them as difficult-to-mine seams [15-19]. After the upper seam is mined, the remaining section pillars form intense stress concentration zones. These pillars are also bounded by caved goaf on both sides, causing the coal drawing law in such seams to differ significantly from that in conventional thick seams. Therefore, determining how to ensure safety and efficiency while achieving a high recovery rate for overlying pillars in steeply dipping, close-proximity seams has become a critical engineering problem that needs to be solved.

To address key issues in top-coal caving, such as improving recovery rate, understanding caving body evolution, and controlling top-coal movement, researchers have conducted extensive studies. These studies have employed methods including numerical simulation, physical modeling, and theoretical analysis, providing important theoretical and practical support for optimizing top-coal caving technology [20-24]. Wei et al. used field measurements to determine the size distribution of coal in an extra-thick seam. Based on this, they combined discrete element numerical calculations and physical experiments to reveal the mixed-motion mechanism of top coal and gangue [25]. Yang et al. focused on the caving mechanism, establishing theoretical models for the drawing body and using PFC3D numerical simulation software to study the caving process under different top-coal caving techniques [26]. Huo et al. employed a coupled Finite Difference Method-Discrete Element Method (FDM-DEM) to simulate the complete caving process over 17 working faces, defining the dynamic evolution of the drawing body (DB), loose body (LB), and top-coal boundary (TCB) [27]. Zhu et al. used random medium theory to derive equations for particle motion and boundaries, creating a theoretical model for calculating top-coal recovery [28]. Sun et al. utilized FLAC and PFC to study the influence of the horizontal distance between the lower roadway and the overlying coal pillar on roadway stability [29]. Wang et al. combined theoretical analysis, 3D physical modeling, and discrete element numerical calculations to study the influence of top-coal particle size distribution on the drawing mechanism [30]. Zhang et al. used experimental and numerical simulation methods to study coal drawing in steeply dipping thick seams [31]. However, a review of the existing literature shows that research has not yet addressed top-coal caving methods for overlying pillars in steeply dipping, extremely close-proximity seams. A systematic study of the drawing laws and the optimization of key process parameters for these specific conditions is still lacking.

This paper addresses the technical challenges of mining steeply dipping, close-proximity seams with an overlying section pillar. An innovative cooperative mining method is proposed for these conditions. First, the FLAC numerical software is used to investigate the optimal horizontal distance for the lower seam roadway. Then, a coupled finite element-discrete element (FLAC-PFC) model is built. This model optimizes the top-coal caving parameters. The study considers the stress evolution of the rock mass and the coal drawing process. It systematically designs and investigates the optimal drawing sequence, caving port width, and recovery method. Finally, the roof deformation, stress distribution, and support loading during drawing are analyzed. The research provides a new methodology for optimizing caving parameters under similar conditions. From a practical standpoint, this work has significant value. It enables the full recovery of steeply dipping, close-proximity coal resources, increases top-coal recovery rates, and helps mitigate stress concentration issues, providing technical support for safe mine production.

2. The case study: mine overview

This study is based on an engineering project at a coal mine in China. The main seams are #1 and #2 coal. The dip angle of the working face ranges from 34° to 45°, with an average of 40°. This classifies it as a steeply dipping, difficult-to-mine seam. The #1 coal is anthracite with high economic value. Its thickness ranges from 3.6 to 4.3 m, with an average of 4.0 m. Due to the seam's steep dip and mining-induced disturbances, a 35 m wide section pillar was left during previous operations.

This resulted in a significant loss of coal resources. The previously mined #1 coal working faces, 1921 and 1922, and the 35 m pillar between them form the core area of this study. The 1921 and 1922 faces had a strike length of approximately 900 m and a dip length of 150 m. They were extracted using the longwall fully mechanized mining method. The #2 coal seam has a thickness of 2.6 to 3.3 m, averaging 3.0 m. The average mining depth is 300 m. This paper focuses on the #2 coal working face 2911. It has a strike length of 920 m and a dip length of 150 m. To recover the resources in the overlying #1 coal pillar, a top-coal caving method is planned for this face. Figure 1 shows the roadway layout and the coal seam columnar section for the 2911 working face.

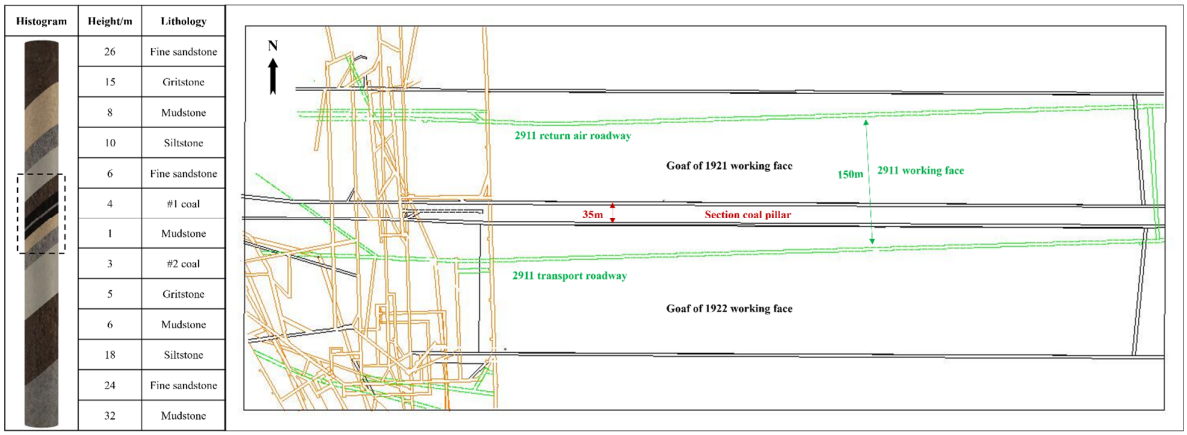

Figure 1. 2911 working face layout and bar chart

The geological characteristics of the #1 and #2 seams were determined from drillhole data, including ZK801. The immediate roof of the #1 coal mainly consists of fine sandstone and siltstone, with secondary layers of mudstone and coarse sandstone. This roof rock is classified as weak and prone to caving. The rock mass integrity is moderate to fractured, with a poor to medium rock mass quality rating. It is considered an unstable roof. The interburden between the #1 and #2 seams is mudstone. It is grayish-white with a slight yellowish tint and has a typical argillaceous structure. The rock has poor integrity and is easily broken. The interburden thickness ranges from 0.6 to 1.3 m, with an average of 1.0 m. The immediate floor of the #2 coal is mainly coarse sandstone. It is grayish-white with a coarse-grained texture. Deeper strata consist of mudstone, siltstone, and fine sandstone.

3. Cooperative mining method and parameter study for large inclination angle and extremely close proximity section coal pillar

3.1. Technical Principle

The core of the cooperative mining method for steeply dipping, close-proximity seams with an overlying pillar is to recover the pillar using a top-coal caving technique while mining the lower seam. The technical principle and system layout are shown in Figure 2.

The system layout features fully mechanized caving supports on one side of the face (under the pillar) and fully mechanized mining supports on the other. This coordinated operation of the caving and mining sections enables the simultaneous extraction of the lower seam and recovery of the overlying pillar. The working face is equipped with a complete set of mining and caving equipment, including a shearer, hydraulic supports, a front armored face conveyor (AFC), a belt conveyor, a stage loader, and a rear AFC for the caving section. All equipment is selected and arranged according to standard top-coal caving practices to minimize interference between the cutting and drawing cycles. To ensure the success of this cooperative method, the mining and caving equipment must operate in a highly coordinated manner, minimizing operational delays. The specific process flow is as follows: Mining Section: The operation follows a cycle of “cut coal, advance hydraulic supports, and advance the front AFC.” Caving Section: The operation follows a cycle of “cut coal, advance caving supports, advance the front AFC, draw top coal (recovering the overlying pillar), and pull the rear AFC.”

This cooperative mining method has strict geological requirements: the interburden thickness between the two seams should generally be less than 1.5 m. This minimizes gangue dilution during drawing and improves the recovery of the overlying pillar. The geological conditions must be

suitable for top-coal caving. The top coal must be able to fracture sufficiently under mining-induced stress. The recovery roadway alongside the pillar must be located outside the pillar's stress concentration zone. This ensures roadway stability and reduces support costs. In steeply dipping seams, the fractured top coal moves under the combined influence of gravity and the seam inclination. It not only flows toward the rear canopy of the support but also slides down the dip of the face. This complex movement creates more complicated loading states and stability challenges for the supports. As a result, support stability becomes a critical factor for ensuring safety. Furthermore, the caving behavior of the pillar, situated between two goaf areas, is more complex than in conventional seams. Therefore, the selection of the drawing method and parameters is crucial for maximizing the final top-coal recovery rate.

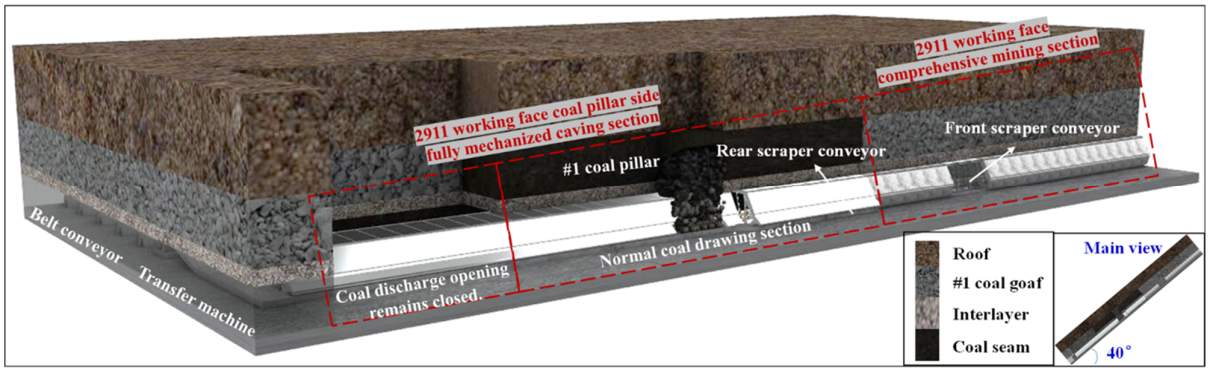

Figure 2. Schematic and system layout of the coordinated mining method for the extremely close-distance coal seam with a steep dip and the overlying section coal pillar

3.2. Study of key Parameter

Based on the actual conditions of the 2911 fully mechanized working face, a 2D numerical model was created using FLAC3D software. The model dimensions were 335 m (length) × 1 m (width) × 323 m (height), representing the actual engineering conditions. The Mohr-Coulomb strength criterion was used for the calculations. Based on in-situ stress measurements, a uniform load of 6.25 MPa was applied to the top of the model to simulate the weight of the overlying strata. The major and minor horizontal stresses were set to 1.3 and 0.72 times the vertical stress, respectively, with the major horizontal stress acting perpendicular to the roadway axis. The model's base was fixed against vertical movement, and the sides were fixed against horizontal movement. The model simulates the prior mining of two 150 m long panels in the #1 coal seam, which created the 35 m wide section pillar. The recovery roadway in the model was designed with dimensions of 4 m wide by 3 m high, matching the site parameters. To further minimize edge effects, a 50 m wide boundary coal pillar was included on all sides of the model area. The primary goal of this model was to find the optimal horizontal distance between the recovery roadway and the overlying pillar. Several scenarios were simulated with different spacing distances. The stability of the roadway in each case was evaluated by analyzing deformation, stress distribution, and the extent of the plastic zone. The mechanical properties for each rock layer in the model were derived from field data and laboratory tests. The GSI and Hoek-Brown criteria were used to scale the laboratory-derived rock properties to the rock-mass scale required for the simulation. The final parameters used in the model are listed in Table 1.

The study investigated the influence of the horizontal distance between the recovery roadway and the section pillar on roadway stability. Four simulation scenarios were designed with spacings of 0 m, 6 m, 12 m, and 18 m. Displacement monitoring lines were placed at locations of maximum deformation in the roof and the pillar-side rib. The simulation results are shown in Figure 3.

Table1. Physical and mechanical Parameter of the rock in each layer of the model

No.	Name	Thickness/m	Density /kg·m^{-3}	Bulk modulus /GPa	Shear modulus /GPa	Cohesion/ MPa	Friction angle /º	Tensile strength /MPa
1	Fine sandstone	26	2600	2.42	1.68	3.49	38	1.34
2	Coarse sandstone	15	2500	2.18	3.01	1.92	32	1.76
3	Mudstone	8	2460	1.12	0.77	1.60	31	0.65
4	Siltstone	10	2400	1.38	1.92	1.99	36	1.50
5	Fine sandstone	6	2600	2.42	1.68	3.49	38	1.34
6	# 1coal seam	4	1400	0.96	0.39	0.36	30	0.24
7	Mudstone	1	2460	1.12	0.77	1.60	31	0.65
8	#2 coal seam	3	1400	0.96	0.39	0.36	30	0.24
9	Coarse sandstone	5	2500	2.18	3.01	1.92	32	1.76
10	Mudstone	6	2460	1.12	0.77	1.60	31	0.65
11	Siltstone	18	2400	1.38	1.92	1.99	36	1.50
12	Fine sandstone	24	2600	2.42	1.68	3.49	38	1.34
13	Mudstone	32	2460	1.12	0.77	1.60	31	0.65

As shown in Figure 3, both vertical and horizontal deformations decrease as the spacing from the pillar increases. Vertical displacement: The maximum vertical displacement decreases from 0.082 m at 0 m spacing to 0.025 m at 6 m. It further reduces to 0.015 m at 12 m and stabilizes at 0.013 m at 18 m spacing. Horizontal displacement: The maximum horizontal displacement decreases from 0.12 m at 0 m spacing to 0.05 m at 6 m. The displacement then stabilizes at 0.02 m for both the 12 m and 18 m spacings. The stress cloud analysis provides further insight. At a spacing of 6 m or less, the roadway is located within the stress concentration zone of the pillar. This high stress causes significant roadway deformation. As the spacing increases to between 12 m and 18 m, the influence of the pillar's stress concentration is reduced, and roadway deformation stabilizes. When the spacing exceeds 18 m, the plastic zone around the roadway is significantly smaller. This greatly improves the overall stability of the surrounding rock mass, which is beneficial for long-term support and maintenance. A combined analysis of displacement, stress distribution, and plastic zone development indicates that a spacing greater than 18 m is optimal. This distance effectively removes the roadway from the pillar's high-stress zone, minimizing deformation and reducing support requirements and costs. Therefore, the optimal horizontal spacing between the recovery roadway and the section pillar was determined to be 18 m.

4. Coal drawing law and parameter optimization design of coal pillar cooperative mining in extremely close section with large inclination angle

4.1. Simulation scheme and model establishment

The FLAC3D model, which simulated the mining of the 1921 and 1922 faces, served as the foundation for this analysis. A coupled finite element-discrete element method was then used. The interburden, the #1 coal pillar, and the immediate roof were converted into a PFC particle flow model. This approach allows for a detailed study of top-coal caving behavior. The overall model is shown in Figure 4. FLAC-PFC coupling is a powerful hybrid computational method. FLAC efficiently models large-scale, continuous rock mass deformation and far-field stress. PFC is embedded in the key area to simulate discontinuous, granular flow. In this study, the key area is the top-coal caving zone. The two codes exchange data on stress, velocity, and displacement at their shared boundary. This method is well-suited for top-coal caving research.

First, the relevant FLAC model elements were converted into PFC discrete particles. The PFC model was then brought to an initial equilibrium state under gravity and in-situ stress. The drawing process was simulated dynamically. Wall elements were used to simulate the opening and closing of a drawing port. Deleting a wall element represents opening a port, while creating one represents its closure. The simulation adopted the "stop when gangue is seen" principle, a common practice in the field. A monitoring zone was established in the model. When roof rock particles were detected in this zone, the current drawing port was closed. The next port in the sequence was then opened. This cycle continued until all recoverable top coal was drawn. A linear model was used for the particle contact calculations. Density was based on laboratory results. Normal and shear stiffness values were determined from previous top-coal caving studies [16]. Particle size was selected to balance accuracy and computational cost. Since the focus is on top-coal drawing, the #1 coal particles were modeled with a smaller diameter. The interburden and roof particles were made larger to

improve computational efficiency. The specific micro-parameters are listed in Table 2.

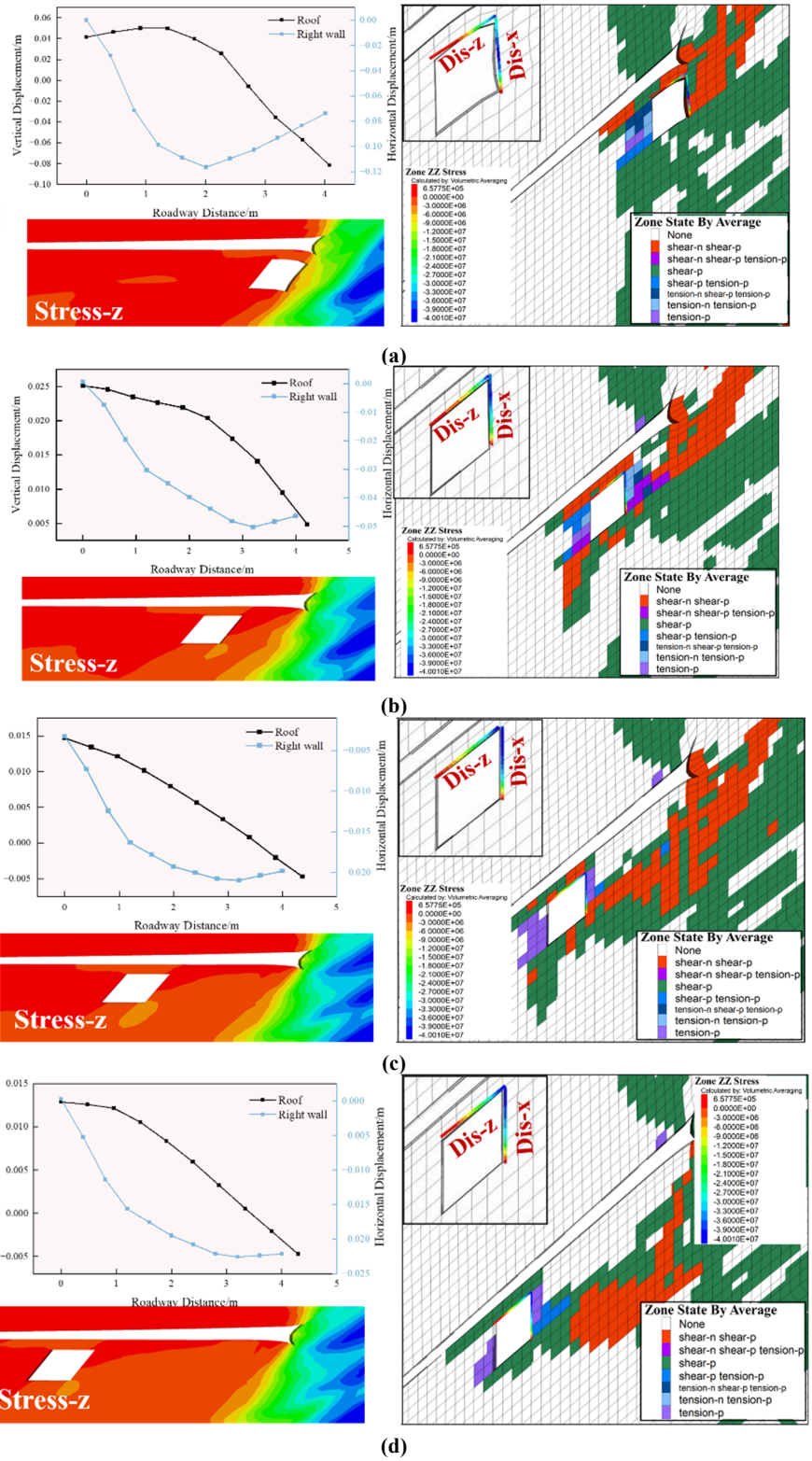

Figure 3. Deformation and Failure Laws of Roadway Surrounding Rock under Different Spacings: (a), (b), (c), (d) represents the spacing is 0m, 6m, 12m, 18m

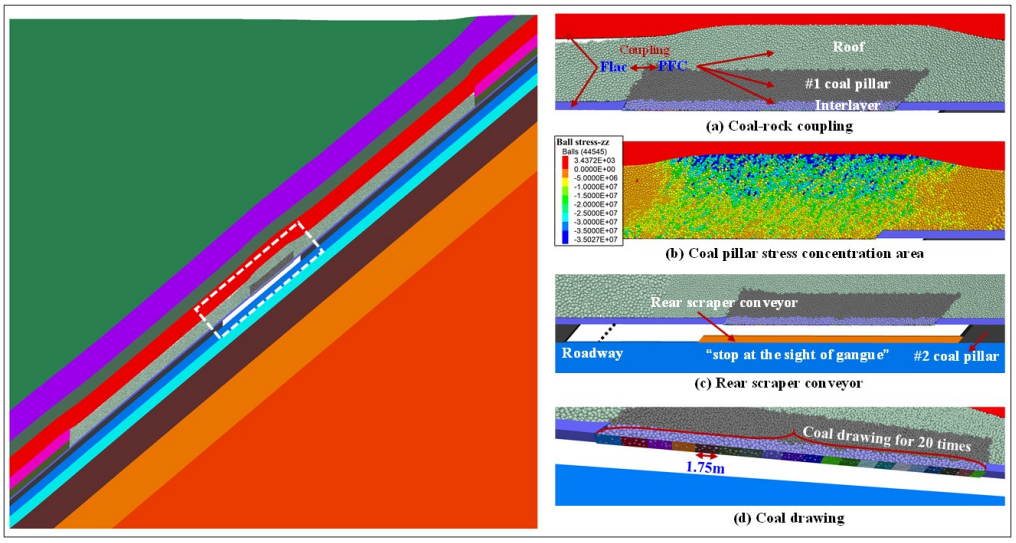

Figure 4. FLAC-PFC Coupled Model

Table 2. Basic Parameter of the coal and rock strata

Strata	Size/mm		Porosity /%	Density /kg m^{-3}	Friction factor	K_n/Pa	K_s/Pa	Gravity acceleration/m s^{-2}
	Minimum	Maximum						
Interlayer	100	200	0.40	2460	0.4	3×10^8	3×10^8	9.8
#1 coal pillar	80	160	0.35	1400	0.4	2×10^8	2×10^8	9.8
Roof	100	200	0.45	2600	0.4	4×10^8	4×10^8	9.8

The optimization study of the top-coal caving process parameters was divided into three stages: Stage 1: Determine the Optimal Drawing Sequence. Two scenarios were designed: "upward drawing" and "downward drawing." To isolate this variable, the port width was fixed at 1.75 m. The drawing method for both was single-round sequential drawing. The optimal sequence was chosen based on coal recovery and gangue content. Stage 2: Determine the Optimal Port Width. In this stage, the optimal drawing sequence from Stage 1 was used as a fixed parameter. The primary focus was to study the effect of port width on drawing performance. Two additional port widths were designed: 1.5 m and 2.0 m. The drawing method remained single-round sequential. By monitoring the coal recovery and gangue content for these new widths and comparing them with the results from the 1.75 m case in Stage 1, the optimal port width was determined. Stage 3: Determine the Final Caving Process Parameters. This stage integrated the results from the first two stages. Based on these findings, the drawing process was further refined to determine the final top-coal caving parameters best suited for the engineering conditions of the working face.

4.2. Optimized design of coal drawing sequence

This study analyzes the particle displacement fields of different drawing sequences to further explain the laws of coal and rock movement. Figures 5(a) and (d) show the displacement fields of the top coal after every five draws for the two sequences (upward and downward drawing). The BBR system, based on the granular media flow theory of top coal, provides the framework for this analysis. The BBR system describes the relationship between the coal-rock interface, the top-coal caving body, and the recovery rate. Studying this system clarifies the top-coal drawing mechanism [20]. Therefore, this paper employs the BBR system to investigate the morphology of the coal-rock interface and the development of the caving body. The ultimate goal is to "increase top-coal recovery and reduce gangue content." FISH functions, a built-in feature of the PFC numerical software, were used to handle complex simulation tasks. To accurately capture the characteristics of the caving body, a FISH function was used to identify the particles drawn during the process and record their trajectories. Particles were regrouped at the beginning of the simulation. Their final positions and shapes were used to map the distribution of the caving body every five draws, as shown in Figures 5(b) and (e). Additionally, to thoroughly evaluate the effectiveness of the drawing process, maps of the residual coal in the goaf were also created. These results are shown in Figures 5(c) and (f).

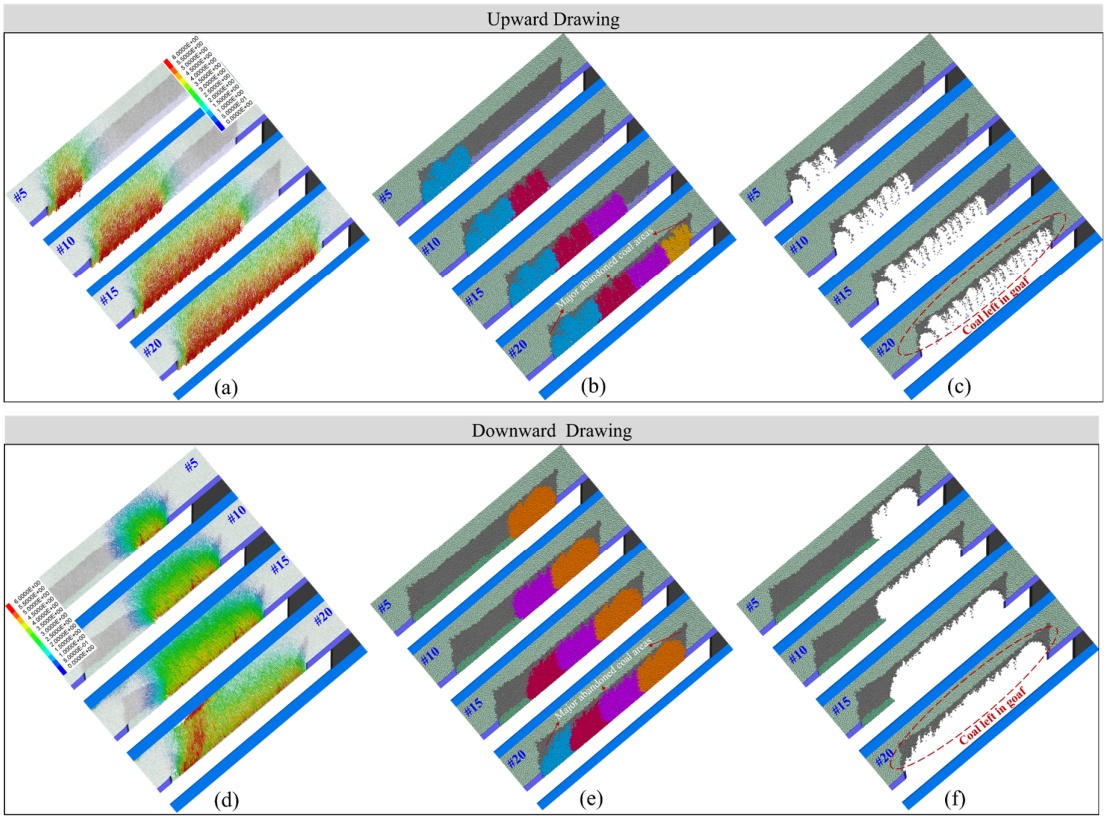

Figure 5. Coal-Rock Movement Characteristics and Caving Body Distribution under different drawing sequences: (a), (d) Displacement Field Distribution; (b), (e) Caving Body Characteristics; (c), (f) Residual Coal Distribution in Goaf

A detailed analysis of Figures 5 reveals the following: Upward Drawing: The displacement flowlines form a small angle with the vertical direction. The distribution is noticeably asymmetrical, centered on the drawing port. Displacement is greater for particles on the right side. The influence range of drawing is also wider. After drawing at ports #5, #10, #15, and #20, the top coal is mobilized at distances of approximately 10.1 m, 8.2 m, 6.9 m, and 5.1 m ahead of the respective ports. The residual coal analysis shows that coal loss is mainly concentrated at the two upper corners of the pillar. Some coal is also lost from the central top portion. Downward Drawing: In contrast, the displacement flowlines are nearly perpendicular to the drawing port. The overall displacement is significantly less than in upward drawing. The range of influence is also narrower. After drawing at ports #20, #15, #10, and #5, the advance mobilization distances are 8.5 m (#20, #15), 6.3 m, and 3.9 m, respectively. These are consistently less than the distances observed in upward drawing. The drawing body analysis indicates that downward drawing results in greater coal loss at the upper corners of the pillar but less loss from the central top portion.

Numerical simulation was employed to study coal recovery and gangue content for both drawing sequences. A FISH function was used to calculate the mass of coal and gangue drawn at each stage. This data was then used to determine the overall recovery rate and gangue content for each sequence. The results are presented in Figure 6. To ensure clarity, the support numbering conventions differ for each sequence: supports are numbered from bottom to top for upward drawing, and from top to bottom for downward drawing. This ensures that the drawing port number always corresponds to the correct support location. Table 3 provides a summary of the key performance indicators.

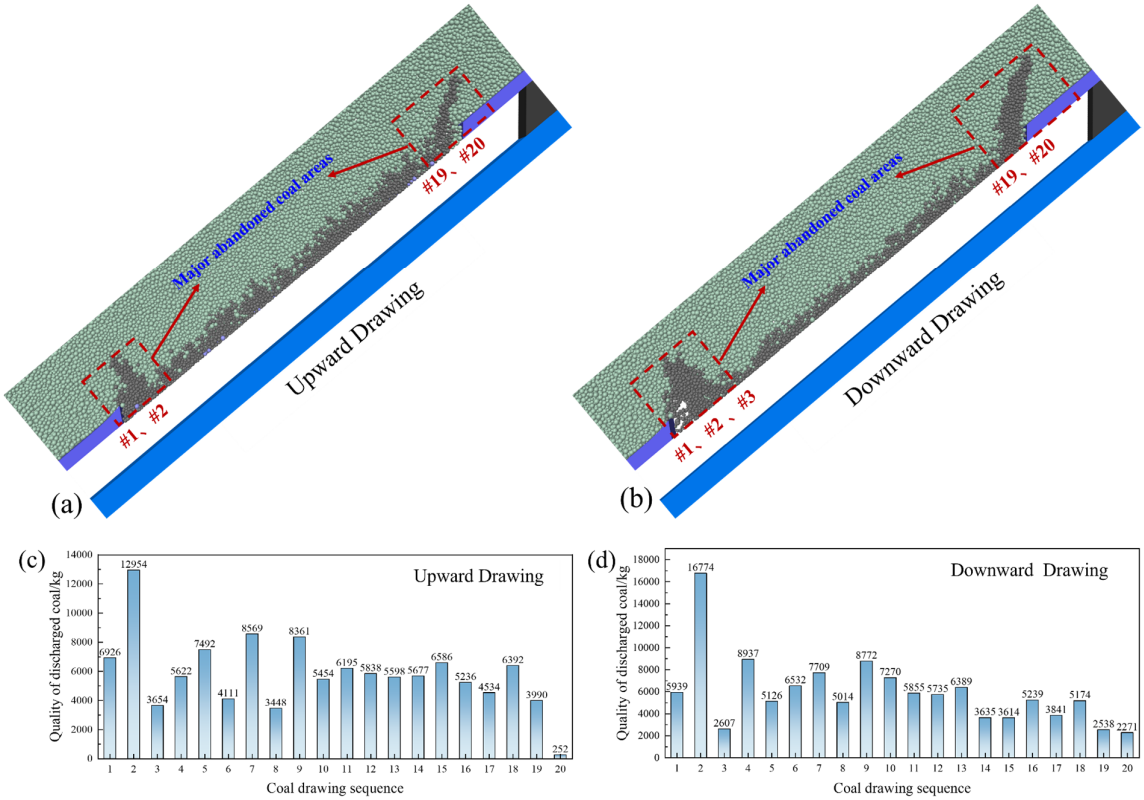

Figure 6. Cloud Maps and Bar Charts of Caving Results for Different Drawing Sequences:(a), (b) Cloud map; (c), (d) Coal mass drawn from each port

Table 3 Statistics of Recovery Rate and Gangue Mixing Ratio for Different Drawing Sequences

Coal drawing sequence	#1 coal pillar total mass	Total mass caving /kg	Drawing mass/kg	Amount of gangue mixed /kg	Drawing ratio /%	Gangue content /%
Upward Coal drawing	152836	125749	116889	8860	76.48	7.05
Downward Coal drawing	152836	122832	118972	3860	77.84	3.14

As shown in Figure 6 and Table 3, in upward drawing, there is less residual coal on the pillar sides, but a significant amount remains in the central upper region. The main residual coal zones are above drawing ports #1, #2, #19, and #20. In downward drawing, more residual coal remains on the sides of the pillar, while the central upper region is more effectively recovered. The main residual coal zones are above ports #1, #2, #3, #19, and #20. The volume of a single draw for both sequences follows a similar pattern: a sharp increase occurs during the second draw, reaching two to three times the average volume. After the second draw, the volume fluctuates but remains relatively stable. From an efficiency and gangue control perspective, upward drawing achieves a coal recovery rate of 76.48% with a gangue content of 7.05%. Downward drawing increases the recovery rate to 77.84% and reduces the gangue content to 3.14%. Based on residual coal distribution, recovery rate, and gangue control, downward drawing is the superior method and will serve as the basis for subsequent optimization studies.

4.3. Optimized design of coal drawing opening width

With the downward drawing sequence established, this study further investigates the effect of different port widths on drawing performance. The simulation results are presented in a series of figures. These figures show the particle displacement field (Figures 7a, d), the caving body shape (Figures 7b, e), and the distribution of residual coal in the goaf (Figures 7c, f).

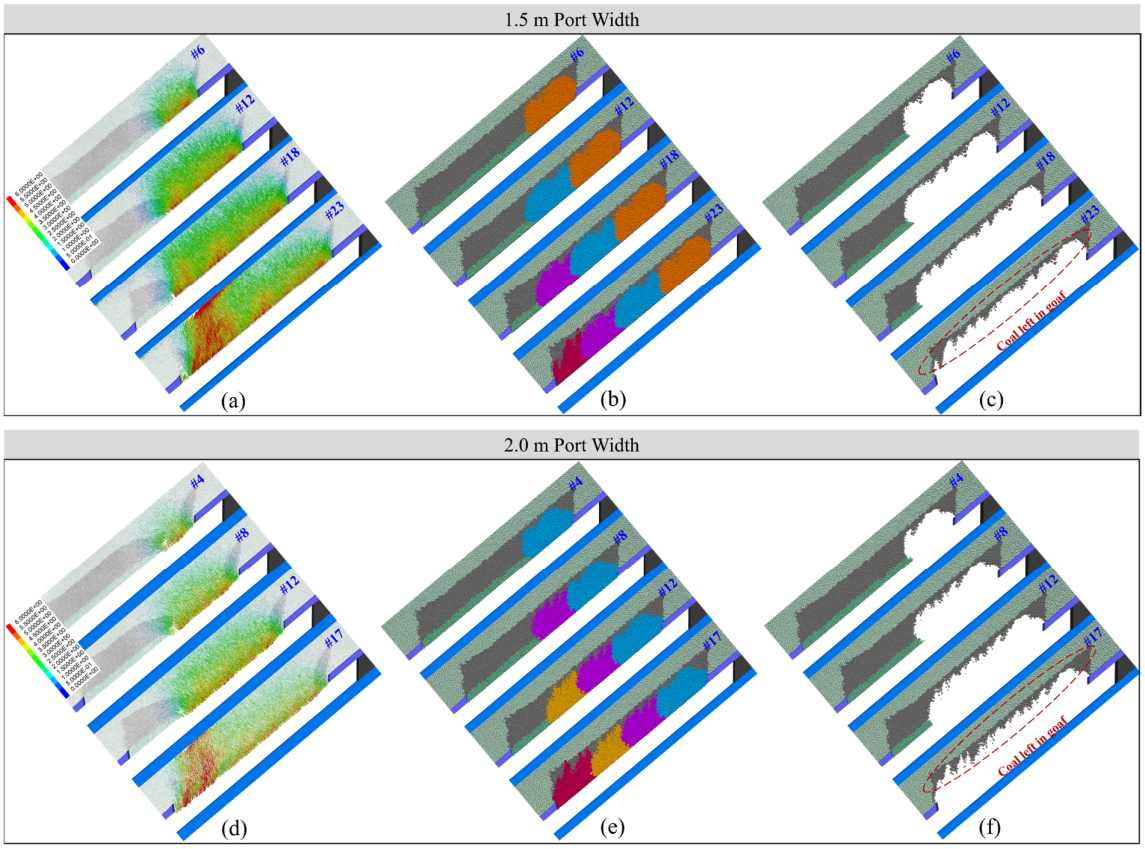

Figure 7. Coal and rock movement characteristics and distribution of drawing bodies for different port widths: (a), (d) Displacement Field Distribution; (b), (e) Caving Body Characteristics; (c), (f) Residual Coal Distribution in Goaf

An analysis of Figures 7 shows that the displacement field pattern is consistent for different port widths under the downward drawing sequence. The displacement flowlines are approximately perpendicular to the drawing port. Only during the final five drawing stages does a local zone of increased displacement appear, caused by particle inflow from the upper right of the pillar. However, there is a significant difference in the advance mobilization range of the top-coal particles. 1.5 m Port Width: After drawing at ports #6, #12, #18, and #23, top-coal particles were mobilized at distances of approximately 6.4 m, 6.3 m, 5.5 m, and 5.2 m ahead of the respective ports. 2.0 m Port Width: After drawing at ports #4, #8, #12, and #17, particles were mobilized at distances of approximately 12.8 m, 6.7 m, 5.2 m, and 3.9 m ahead. The overall results show a clear principle: a wider port creates a larger average zone of influence on the top coal during drawing.

Based on an analysis of the caving body shape, the drawing process was divided into stages of 4 to 6 ports. It was found that, for all port widths, the volume drawn in each stage shows a sequentially decreasing trend. The stage consisting of the first five ports yields the highest total volume, while the stage of the last five ports yields the lowest. The distribution of residual coal in the goaf also varies significantly with port width. With a 1.5 m width, the most residual coal is in the upper-left corner of the goaf. With a 1.75 m width, the amount of residual coal is roughly balanced between the upper-left and upper-right corners. With a 2.0 m width, the most residual coal is in the upper-right corner.

To quantify the effect of port width on drawing performance, a numerical study was conducted on the coal recovery rate and gangue content for 1.5 m and 2.0 m port widths. It should be noted that the number of drawing ports differs between the two scenarios: the 1.5 m width simulation has 23 ports, while the 2.0 m width has 17. Figure 8 shows the cloud diagrams of the drawn coal and the total mass recovered from each port for both widths. The total recovery and gangue content for each scenario are summarized in Table 4.

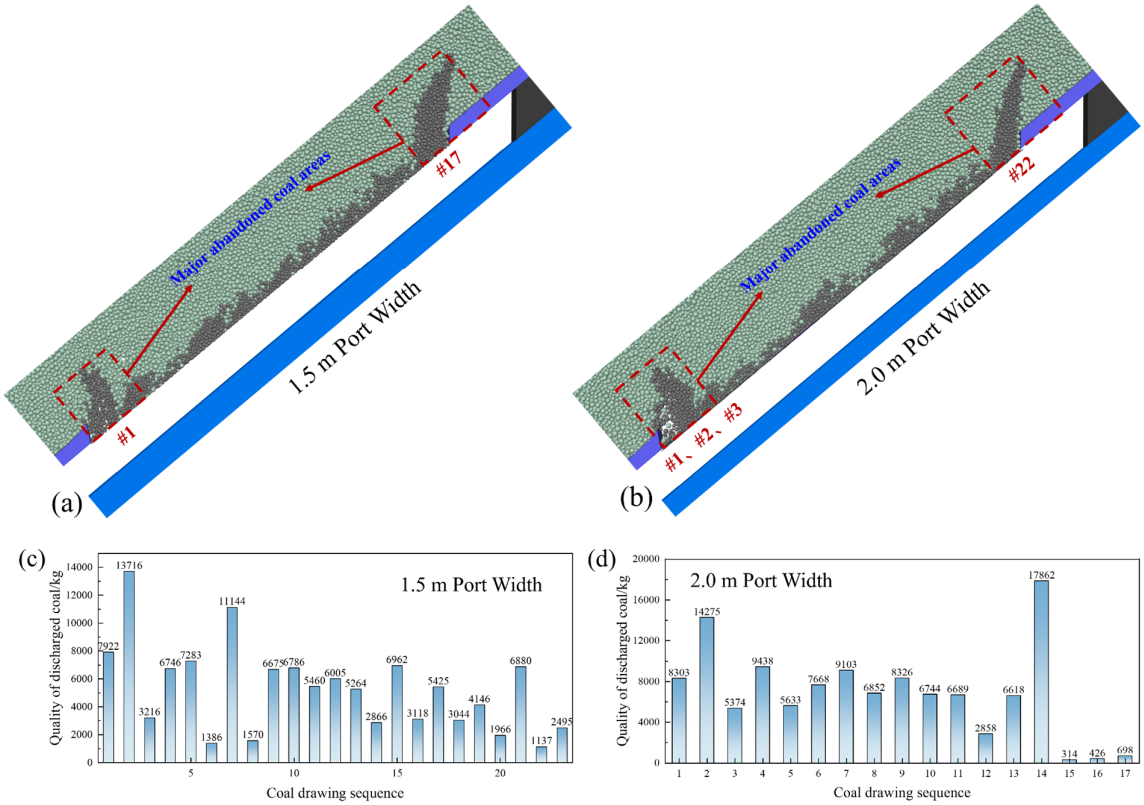

Figure 8. Cloud diagram and bar chart of coal drawing results for different port widths: (a), (b) Cloud diagram; (c), (d) Coal mass drawn from each port

Table 4 Statistics of Recovery Rate and Gangue Mixing Ratio for different widths of coal drawing openings

Drawing opening dimension	#1 coal pillar total mass	Total mass caving /kg	Drawing mass/kg	Amount of gangue mixed /kg	Drawing ratio /%	Gangue content /%
1.5m	152836	124792	121212	3580	79.31	2.87
2.0m	152836	121124	117184	3940	76.67	3.36

With a 1.5 m width, more residual coal is left on the left side of the pillar. The main zones of lost coal are above ports #1, #2, #3, and #22. With a 2.0 m width, more residual coal is left on the right side of the pillar. The main zones are located above ports #1 and #17. The pattern of coal volume drawn from a single port also differs significantly between the two cases: with a 1.5 m width, the volume drawn from each port is relatively uniform. The maximum volume occurs during the second draw. With a 2.0 m width, the maximum draw volume occurs at the 14th draw. The final three draws yield almost no coal, and the ratio of the maximum to minimum draw volume is as high as 56.89. In conclusion, based on a combined analysis of recovery rate and gangue content, the 1.5 m port width was selected as the basis for subsequent optimization of the caving process parameters.

4.4. Optimized design of coal drawing method

To further optimize the top-coal caving process, this study compares the drawing effects of two different drawing methods: single-round interval drawing and two-round sequential drawing. The particle displacement fields for each method are shown in Figures 9(a) and (d). The caving body morphology is presented in Figures 9(b) and (e), and the distribution of residual coal in the goaf is illustrated in Figures 9(c) and (f).

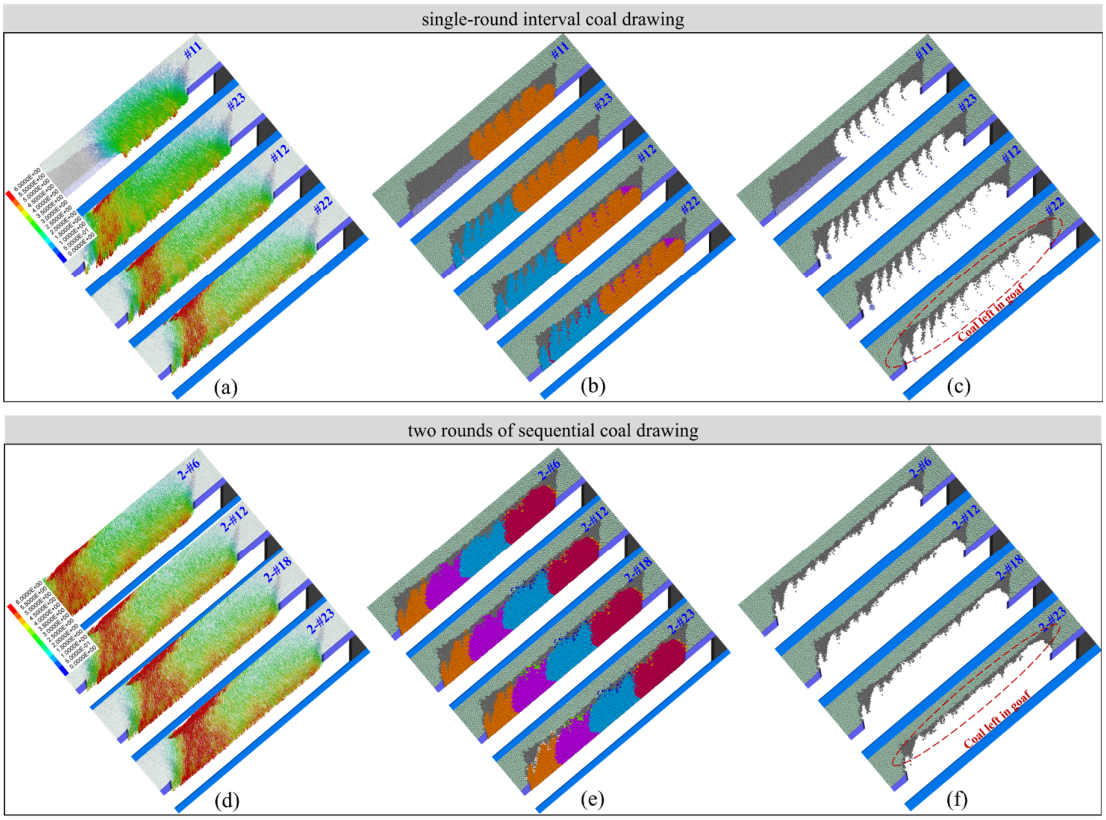

Figure 9. Characteristics of coal rock movement and distribution of drawing bodies for different drawing methods: (a), (d) Displacement Field Distribution; (b), (e) Caving Body Characteristics; (c), (f) Residual Coal Distribution in Goaf

Analysis of Single-Round Interval Drawing: During the first draw, there are noticeable differences in displacement. Odd-numbered drawing ports show greater particle displacement than even-numbered ports. The cloud diagram of the caving body shows an elliptical shape, with its major axis forming an angle of approximately 50° with the drawing port. A significant portion of the coal is drawn during the first stage. However, during the second draw, the ingress of roof gangue limits the recovery to only a small part of the top coal. This results in a substantial amount of residual coal in the middle section of the pillar. Additionally, after the odd-numbered ports complete drawing, the top coal above the even-numbered ports is difficult to recover effectively.

In contrast to single-round interval drawing, the two-round sequential drawing process exhibits different characteristics and effects. During the second round of drawing, the overall change in the displacement field is less pronounced. This is because the first round of drawing has already caused roof caving. The resulting mixture of fallen roof gangue and unrecovered coal restricts the amount of coal that can be drawn in the second round. Despite this limitation, the two-round sequential drawing method achieves a significantly higher total recovery rate. Furthermore, the gangue content remains at a low level.

To quantitatively compare the drawing effectiveness of single-round interval drawing and two-round sequential drawing, a study was conducted on the coal recovery rate and gangue content for both methods. First, the specific operating procedures for each method are defined: Single-Round Interval Drawing: This method uses a “first odds, then evens” sequence. Drawing begins at port #23, then proceeds to #21, #19, and so on. After all odd-numbered ports are drawn, the process continues with the even-numbered ports: #22, #20, #18, etc. Two-Round Sequential Drawing: This method uses a “two-round continuous” approach. The first round of drawing proceeds sequentially through all ports. A second round of drawing then follows the same numerical order. The cloud diagrams of the drawn coal and the total mass recovered from each port are shown in Figure 10. The total recovery and gangue content for each method are summarized in Table 5.

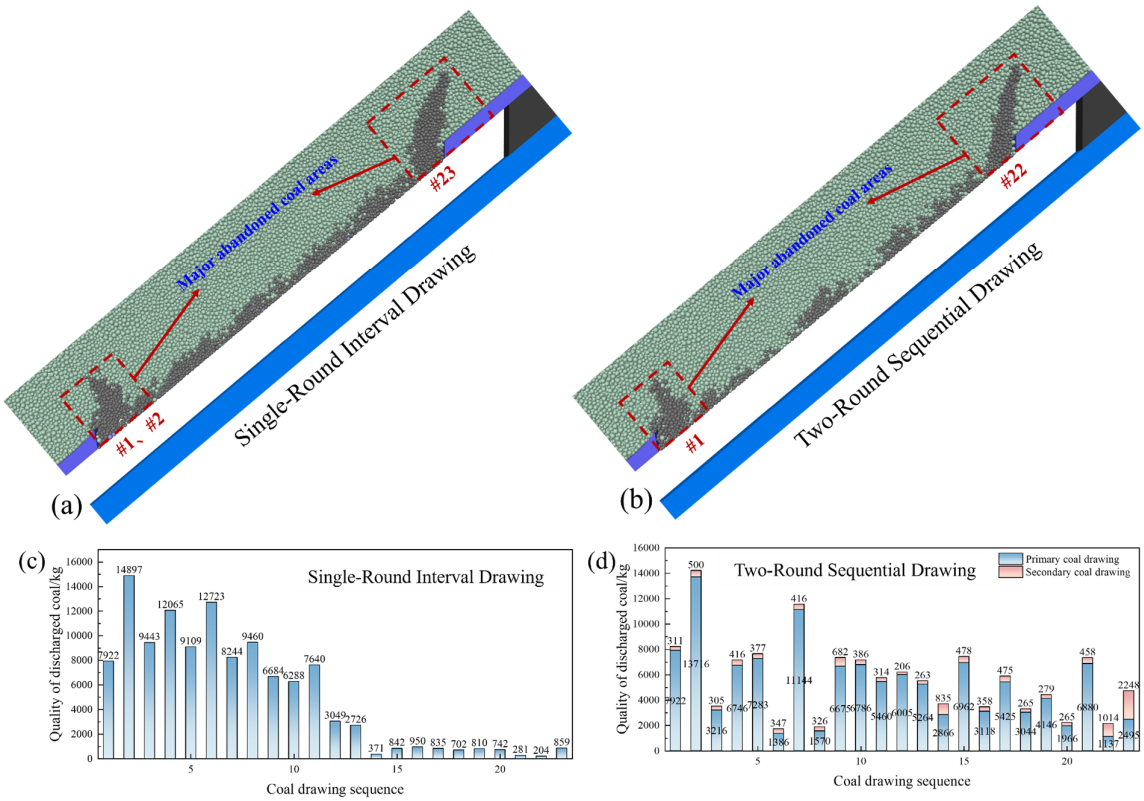

Figure 10. Cloud diagram and bar chart of coal drawing results for different coal drawing methods: (a), (b) Cloud diagram; (c), (d) Coal mass drawn from each port

Table 4 Statistics of Recovery Rate and Gangue Mixing Ratio for different coal drawing methods

Coal drawing method	#1 coal pillar total mass	Total mass caving /kg	Drawing mass/kg	Amount of gangue mixed /kg	Drawing ratio /%	Gangue content /%
Single-wheel interval coal drawing	152836	119906	116846	3060	76.45	2.55
Sequential coal drawing with two wheels	152836	137182	130858	6324	85.62	4.61

From the residual coal analysis, the main zones of lost coal in the single-round interval method are above ports #1, #2, and #23. A review of the bar chart in Figure 13 shows a significant imbalance in the drawing volume for this method. The first interval draw recovers a large portion of the coal, accounting for 92.02% of the total. The second interval draw yields a much smaller volume. The coal recovery for this method is 76.45%, with a gangue content of 2.55%. This recovery rate is lower than that of the single-round sequential method, indicating that while interval drawing controls gangue content, it also limits overall resource recovery.

In contrast, the residual coal in the two-round sequential drawing method is mainly concentrated above ports #1 and #22. A much larger portion of the top coal from the middle section of the pillar is recovered. The drawing volume is also concentrated in the first round, which accounts for 88.36% of the total. A comparison with the single-round sequential drawing shows that more residual coal is left in the upper-left corner of the pillar. Therefore, in the second round of drawing, the volumes recovered from ports #1 and #2 are the highest. The coal recovery rate for two-round sequential drawing reaches 85.62%, with a gangue content of 4.61%. This recovery rate is significantly higher than that of single-round interval drawing, and the gangue content remains below 5%. This method achieves a good balance between “high recovery” and “low gangue content.”

Based on a multi-dimensional comparison of drawing sequence, port width, and drawing method, the optimal top-coal caving process is determined to be: choosing the downward coal drawing sequence with a coal drawing opening width of 1.5 m and two-round sequential drawing as the optimal coal drawing method. This

combination of parameters achieves a coal recovery rate of 85.62% and a gangue content of 4.61%. While this optimized process meets the engineering requirements, the numerical simulation shows that a significant amount of residual coal remains in the upper two corner areas of the pillar. This issue could be addressed by accepting a higher gangue content to recover the corner coal. Methods such as multiple drawing cycles at the end ports or modifying the "stop when gangue is seen" rule could be used to recover the top triangular coal wedges. However, these methods were not investigated in this study.

Based on the optimized top-coal caving process, further study was conducted on roof deformation and stress distribution for the 1915 and 1916 working faces. The changes in stress and displacement in the roof above both working faces were monitored. Figure 11(a) and (c) show the changes during the first round of drawing at ports #6, #12, #18, and #23. Figure 11(b) and (d) show the changes during the second round of drawing at the same ports. It should be noted that the displacement was zeroed after the initial excavation of the 1915 and 1916 faces. Monitoring began with the first draw of the pillar.

5. Discussion

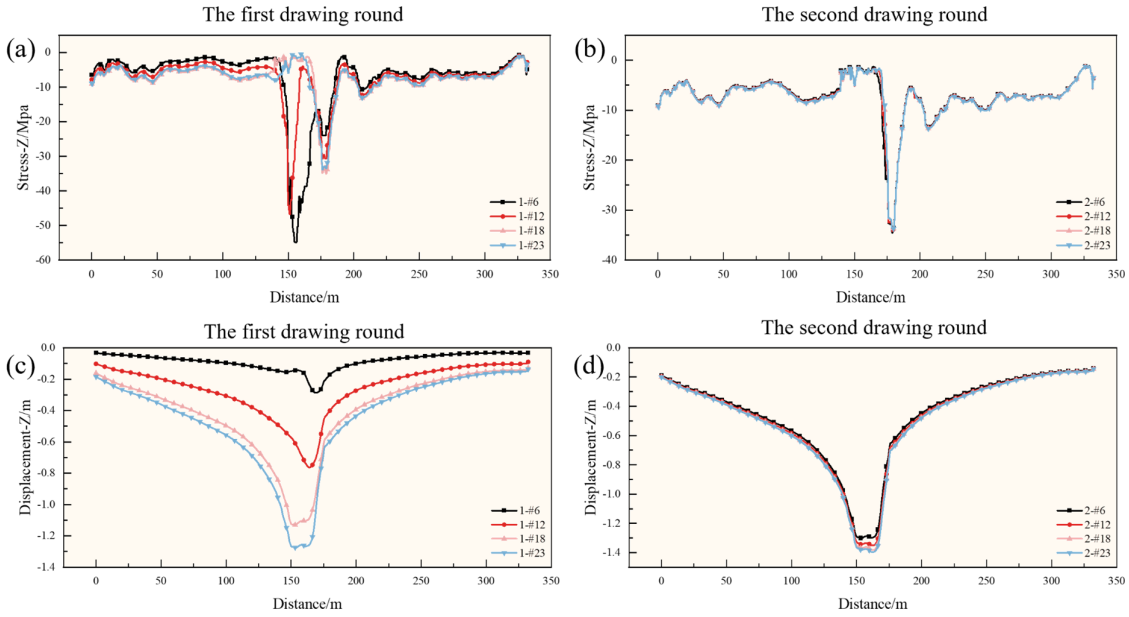

Figure 11. Deformation and stress distribution characteristics of the roof during pillar caving and drawing: (a), (b) Roof stress change; (c), (d) Roof displacement change

Figure 11 shows that during the first round of drawing, the concentrated stress in the roof decreases as the pillar is gradually drawn. After the 6th, 12th, 18th, and 23rd draws, the maximum concentrated stress in the roof above the pillar is 54.9 MPa, 46.7 MPa, 35.0 MPa, and 33.8 MPa, respectively. This shows a significant reduction in stress, with a maximum decrease of 21.1 MPa. This effectively mitigates the high-stress concentration and reduces the safety risks for the working face. During the second round, because less coal is drawn, the concentrated stress remains relatively stable, with the maximum value around 34 MPa. The roof displacement analysis shows that during the first round of drawing, the roof subsidence increases significantly as the pillar is drawn. After the 6th, 12th, 18th, and 23rd draws, the maximum roof subsidence is 0.29 m, 0.76 m, 1.13 m, and 1.27 m, respectively. During the second round, the roof subsidence changes little. After the completion of the second round, the maximum roof subsidence is approximately 1.4 m.

Based on the optimized top-coal caving process, the support loads during the drawing process on the 2911 working face were also studied. The face is 150 m long, with a total of 100 supports. Of these, 35 are fully mechanized caving supports, and 65 are fully mechanized mining supports. The changes in support load during the first round of drawing at ports #6, #12, #18, and #23 are shown in Figure 12.

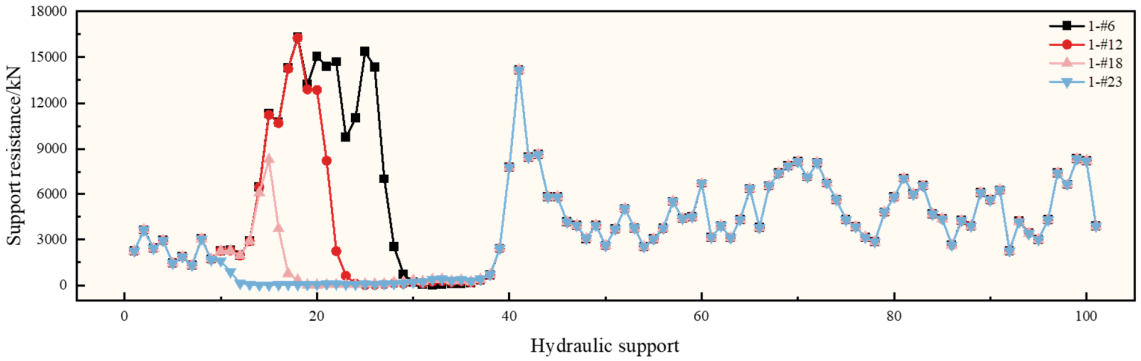

Figure 12. Change curve of the force on the hydraulic support of the coal pillar

Figure 12 shows that during the first round of drawing, the maximum total load on the caving supports gradually decreases as the pillar is drawn. After drawing at ports #6, #12, #18, and #23, the maximum load on the supports is approximately 1.6×10^4 KN, 1.6×10^4 KN, 0.8×10^4 KN, and 100 KN, respectively. After the first round, the roof has not completely caved, so the load on the caving section supports is relatively low. The maximum load on the fully mechanized mining supports is approximately 1.4×10^4 KN. This load is located on the side near the pillar. The total load on the other mining supports is relatively stable, with a maximum of only 8000 KN. This analysis of support load changes can provide a reference for support selection.

6. Conclusions

(1) A cooperative mining method was proposed for steeply dipping, closely spaced seams with an overlying section pillar, employing a top-coal caving technique to recover the pillar while mining the lower seam. Numerical simulations were conducted to analyze the effect of the roadway-pillar distance on roadway stability. The results indicate that as the distance increases from 0 m to 18 m, roadway stability improves, with maximum vertical displacement decreasing and horizontal displacement being reduced by 0.1 m. At 18 m, the roadway is effectively outside the pillar's stress concentration zone, which mitigates high-stress effects, minimizes the surrounding plastic zone, and reduces the difficulty and cost of support. Therefore, 18 m was determined to be the optimal distance between the roadway and the pillar.

(2) A coupled FLAC-PFC numerical simulation was used to optimize the top-coal caving process parameters. For the drawing sequence, downward drawing proved superior to upward drawing, increasing the recovery rate to 77.84% and reducing gangue content to 3.14%. Based on this, a port width of 1.5 m was found to be optimal, achieving a 79.31% recovery rate and 2.87% gangue content, outperforming the 2.0 m width. Finally, two-round sequential drawing significantly increased the recovery rate to 85.62% with a gangue content of 4.61%, proving more effective than single-round interval drawing. A comprehensive analysis identified the optimal process: a downward drawing sequence, a 1.5 m port width, and two-round sequential drawing.

(3) Based on the optimized process, the roof behavior and support loading during pillar caving were analyzed. Roof Stress Evolution: The first drawing round significantly reduced roof stress concentration, with a maximum decrease of 21.1 MPa, effectively mitigating high stress. During the second round, as only residual coal was recovered, roof stress remained stable at approximately 34 MPa. This demonstrates that drawing the pillar effectively reduces roof stress and associated safety risks. Roof Deformation: The maximum roof subsidence reached 1.27 m after the first round. The process concluded with a total maximum subsidence of approximately 1.4 m, an increase of only 0.13 m during the second round. This indicates the optimized process effectively controls final roof deformation. Support Loading: The maximum total loads on the caving and mining supports were recorded as 1.6×10^4 kN and 1.4×10^4 kN, respectively, providing a crucial reference for support selection and design.

(4) Limitations and Practical Implications: While this technology shows promise for high resource recovery and stress mitigation, it has specific limitations. It requires strict geological conditions, such as an interburden thickness of less than 1.5 m, to control gangue content. Furthermore, ensuring support stability in steeply dipping seams is a major challenge, demanding robust equipment and support systems. The recovery of residual coal in the upper triangular sections of the pillar also requires further optimization. Despite these challenges, the technology's practical implications are substantial. It effectively addresses resource waste and stress concentration caused by leaving large pillars. By increasing coal recovery and mitigating roof stress, it offers a feasible technical path and theoretical

support for efficient and safe extraction under similar complex geological conditions.

References

[1]. Abdollahi, M. S., Najafi, M., Yarahamdi Bafghi, A., et al. (2024). A new method for stability analysis of chain pillar in longwall mining by using coulmann graphical method. *Journal of Mining and Environment, 15*(4), 1461-1476.

[2]. Najafi, M., Jalali, S. M., Sereshki, F., et al. (2016). Probabilistic analysis of stability of chain pillars in Tabas coal mine in Iran using Monte Carlo simulation.

[3]. Ma, L., Liu, C., Zhao, G. (2024). Study on Coal Pillar Setting and Stability in Downward Mining Section of Close Distance Coal Seam. *Energies, 17*(21), 5441.

[4]. Teng, F., Yu, M., Chao, J., et al. (2022). Coal pillar's breaking and fracture development mechanism and numerical simulation. *Thermal Science, 26*(3 Part B), 2439-2446.

[5]. Bu, Q., Tu, M., Fu, B. (2021). Research on the redistribution law of lateral mining stress and the bearing characteristics of section coal pillar in extra‐thick fully mechanized top‐coal caving mining. *Shock and Vibration, 2021*(1), 4355977.

[6]. Najafi, M., Jalali, S. M. E., Sereshki, F., et al. (2016). Probabilistic analysis of stability of chain pillars in tabas coal mine in iran using monte carlo simulation. *Journal of Mining and Environment,7*, 25-35.

[7]. Ghasemi, E., Ataei, M., Shahriar, K. (2014). An intelligent approach to predict pillar sizing in designing room and pillar coal mines. *International Journal of Rock Mechanics & Mining Sciences, 65*(75 (Pt 2)), 86-95.

[8]. Ghasemi, E., Ataei, M., Shahriar, K. (2014). Prediction of global stability in room and pillar coal mines. *Natural Hazards 72*(2), 405-422.

[9]. Kunkyin-Saadaari, F., Offei, J. B., Sadique, S. I., et al. (2025). Investigating the Applicability of Stacked Generalization Technique for the Prediction of Hard Rock Pillar Stability Status. *Journal of Mining and Environment, 16*(3), 907-923.

[10]. Sarfarazi, V., Karimi Javid, H., Asgari, K. (2021). Study of rock pillar failure consisting of non-persistent joint using experimental test and fracture analysis code in two dimensions. *Journal of Mining and Environment, 12*(1), 163-179.

[11]. Rezaei, A., Sarfarazi, V., Babanouri, N., et al. (2023). Failure Mechanism of Rock Pillar Containing Two Edge Notches: Experimental Test and Numerical Simulation. *Journal of Mining and Environment, 14*(3), 961-971.

[12]. Ardehjani, E. A., Ataei, M., Sereshki, F., et al. (2024). Examining the impact of coal gas emissions on the stability analysis of coal pillars: a critical literature review. *Rudarsko-Geolosko-Naftni Zbornik, 39*(3). DOI: 10.17794/rgn.2024.3.7, Vol. 39 No. 3 (2024): No. 69, PP. 77-94.

[13]. Ansari Ardehjani E., Ataei M., Sereshki F. (2025). Impact of CO2 and Methane Adsorption and Emission on Coal's Mechanical Properties and Pillar Stability: Implications for ECBM and CO2 Sequestration, *Energy, 333 137438*, DOI: 10.1016/j.energy.2025.137438.

[14]. Abdollahi, M. S., Najafi, M., Yarahamdi Bafghi, A., et al. (2024). A New Method for Stability Analysis of Chain Pillar in Longwall Mining by using Coulmann Graphical Method. *Journal of Mining and Environment, 15*(4), 1461-1476.

[15]. Yang, S. L., Li, Q., Yue, H., et al. (2024). Study on Roof Deformation and Failure Law of Close Distance Coal Seams Mining Based on Digital Image Correlation. *Experimental Techniques, 48*(6), 1005-1026.

[16]. Wei, X. Q., Bai, H. B., Rong, H. R., et al. (2011). Research on mining fracture of overburden in close distance multi-seam. *Procedia Earth and Planetary Science, 2*, 20-27.

[17]. Zhang, W., Zhang, D., Qi, D., et al. (2018). Floor failure depth of upper coal seam during close coal seams mining and its novel detection method. *Energy Exploration & Exploitation, 36*(5), 1265-1278.

[18]. Li, X., Liu, Y., Ren, X., et al. (2023). Roof breaking characteristics and mining pressure APPEARANCE laws in close distance COAL seams. *Energy Exploration & Exploitation, 41*(2), 728-744.

[19]. Zhang, J., Zhuo, Q., Yang, S., et al. (2022). Study on the coal pillar weakening technology in close distance multi-coal seam goaf. *Energies, 15*(18), 6532.

[20]. Zhang, J., Cheng, Z., Lei, S., et al. (2025). Research on the Law of Top Coal Movement and Influence Factors of Coal Caving Ratio for Fully Mechanized Top Coal Caving Working Face. *Energies, 18*(16), 4312.

[21]. Liang, M., Hu, C., Yu, R., et al. (2022). Optimization of the process parameters of fully mechanized top-coal caving in thick-seam coal using BP neural networks. *Sustainability, 14*(3), 1340.

[22]. Liu, C., Li, H. (2021). Numerical simulation of realistic top coal caving intervals under different top coal thicknesses in longwall top coal caving working face. *Scientific Reports, 11*(1), 13254.

[23]. Zhang, Q. L., Yue, J. C., Liu, C., et al. (2019) Study of automated top-coal caving in extra-thick coal seams using the continuum-discontinuum element method. *International Journal of Rock Mechanics and Mining Sciences 122*:104063.

[24]. Wang, J. C., Zhang, J. W., Li, Z. L. (2016) A new research system for caving mechanism analysis and its application to sublevel top-coal caving mining. *International Journal of Rock Mechanics and Mining*

Sciences 88:273-285.

[25]. Wei, W. J., Yang, S. L., Li, M., et al. (2022) Motion mechanisms for top coal and gangue blocks in longwall top coal caving (LTCC) with an extra-thick seam. *Rock Mechanics and Rock Engineering 55*(8):5107-5121.

[26]. Yang, S. L., Wei, W. J., Yang, L., et al. (2024). Theoretical investigation and key caving technology development at the end area of longwall top coal caving (LTCC) panels. *Computational Particle Mechanics, 11*(1), 235-247.

[27]. Huo, Y., Zhu, D., Wang, Z., et al. (2021). Numerical Investigation of Top Coal Drawing Evolution in Longwall Top Coal Caving by the Coupled Finite Difference Method-Discrete Element Method. *Energies, 14*(1), 219.

[28]. Zhu, D., Chen, Z., Du, W., et al. (2018). Caving mechanisms of loose top-coal in longwall top-coal caving mining based on stochastic medium theory. *Arabian Journal of Geosciences, 11*(20), 621.https://doi.org/10.1007/s12517-018-3987-3

[29]. Sun Q., Gao J. L., Yang F., et al. (2023). Cooperative mining technology and strata control of close coal seams and overlying coal pillars. *Alexandria Engineering Journal, 73*, 473-485.

[30]. Wang, J., Wei, W., Zhang, J. (2019). Effect of the size distribution of granular top coal on the drawing mechanism in LTCC. *Granular Matter, 21*(3), 70.

[31]. Zhang, J. W., Wang, J. C., Wei, W. J., et al. (2018). Experimental and numerical investigation on coal drawing from thick steep seam with longwall top coal caving mining. *Arabian Journal of Geosciences, 11*(5), 96.

انجمن مهندسی معدن ایران
نشریه مهندسی معدن و محیط زیست
نشانی نشریه: www.jme.shahroodut.ac.ir
دانشگاه صنعتی شاهرود

استخراج مشارکتی ستون‌های زغال‌سنگ مقطع رویی در رگه‌های زغال‌سنگ با شیب تند و بسیار نزدیک: یک بررسی عددی

فنگ یانگ[۱]، پنگجی لی[۱*] و کیانگ سان[۱،۲]

۱. دانشکده معادن، دانشگاه معدن و فناوری چین، شوژو ۲۲۱۱۱۶، چین
۲. آزمایشگاه کلیدی ایالتی برای مهندسی ژئومکانیک و اعماق زمین، دانشگاه معدن و فناوری چین، شوژو ۲۲۱۱۱۶، چین

اطلاعات مقاله

تاریخ ارسال: ۲۰۲۵/۰۷/۳۰
تاریخ داوری: ۲۰۲۵/۱۰/۱۲
تاریخ پذیرش: ۲۰۲۶/۰۱/۱۰

DOI:10.22044/jme.2026.16570.3246

کلمات کلیدی

خاکستر بادی
بنتونیت، الیاف شیشه
مقاومت فشاری تک محوری
ضریب نفوذپذیری

چکیده

ستون‌های بزرگ زغال‌سنگ منجر به اتلاف قابل توجه منابع می‌شوند. تمرکز بالای تنش در این ستون‌ها همچنین خطرات ایمنی را برای جبهه کار ایجاد می‌کند. برای رسیدگی به این موضوع، یک روش استخراج مشارکتی برای ستون‌های زغال‌سنگ مقطعی پیشنهاد شده است. این روش برای درزهایی با زاویه شیب بزرگ و بسیار نزدیک به ستون‌های رویی طراحی شده است. اصول فنی توضیح داده شده است. ابتدا، از نرم‌افزار شبیه‌سازی FLAC3D برای بررسی تأثیر فاصله بین جاده پایینی و ستون زغال‌سنگ مقطعی استفاده شد که موقعیت بهینه جاده را تعیین کرد. سپس، از یک روش کوپل شده FLAC-PFC برای بهینه‌سازی پارامترهای فرآیند کشش زغال‌سنگ استفاده شد. طرح بهینه برای توصیف تغییر شکل سقف، توزیع تنش و بارهای پشتیبانی هیدرولیکی مورد تجزیه و تحلیل قرار گرفت. یک مطالعه موردی مهندسی نشان می‌دهد که فاصله بیش از ۱۸ متر، تأثیر تنش متمرکز را به حداقل می‌رساند و منجر به تغییر شکل محدود و بهبود پایداری جاده می‌شود. این مطالعه کشش زغال‌سنگ را تحت توالی‌ها، عرض‌های دریچه و روش‌های مختلف بررسی می‌کند. فرآیند بهینه به عنوان کشش رو به پایین، با عرض دریچه کشش زغال‌سنگ ۱.۵ متر و روش متوالی دو چرخ شناسایی شد. این فرآیند به نرخ کشش ٪۸۵.۶۲ و میزان گانگ ٪۴.۶۱ دست می‌یابد. تجزیه و تحلیل نشان می‌دهد که در طول فرآیند کشش ستون، تنش متمرکز روی صفحه سقف به طور قابل توجهی کاهش می‌یابد، با حداکثر کاهش تنش ۲۱.۱ مگاپاسکال، که به طور موثر تمرکز تنش را کاهش می‌دهد. نیروی کل وارد بر تکیه‌گاه هیدرولیکی بخش در حفاری کاملاً مکانیزه ۱.۶×۱۰^4 کیلونیوتن است، در حالی که این نیرو در بخش استخراج کاملاً مکانیزه ۱.۴×۱۰^4 کیلونیوتن است.

نویسنده مسئول مکاتبات: lipengjie@cumt.edu.cn (پ. لی)